Principal Modes of Outgoing Longwave Radiation and 250-mb Circulation for the South American Sector

VERNON E. KOUSKY

Climate Analysis Center, NOAA/NWS/NMC, Washington, D.C.

MARY T. KAYANO*

Instituto Nacional de Pesquisas Espaciais, Centro de Previsão de Tempo e Estudos Climaticos, São José dos Campos, São Paulo, Brazil

(Manuscript received 13 May 1992, in final form 11 November 1993)

ABSTRACT

Principal modes of anomalous upper-tropospheric circulation and outgoing longwave radiation (OLR) are determined for the South American sector. A combined EOF analysis is performed using anomalous 250-mb zonal and meridional wind components plus anomalous OLR. The data are filtered so that modes on both intraseasonal and interannual timescales can be studied separately. The resulting patterns show a consistent relationship between anomalous OLR and anomalous upper-tropospheric circulation features.

The first and second interannual modes contain many atmospheric features related to extremes in the Southern Oscillation. These include 1) variations in the pattern of tropical convection, and 2) changes in the intensity of upper-tropospheric zonal flow in the equatorial band and in the subtropics. The first intraseasonal mode has its greatest loadings in the Tropics and is most active during the southern summer season. For positive (negative) amplitudes of this mode, anomalous upper-tropospheric westerly (easterly) flow dominates the Tropics throughout the region, and positive (negative) OLR anomalies are observed over northeastern South America and over the eastern equatorial Pacific. These features are associated with the 30–60 day (Madden–Julian) oscillation.

An extended combined EOF analysis was performed to study the evolution of intraseasonal oscillations in the South American sector. The first rotated combined extended EOF mode describes a sequence of patterns in which anomalous equatorial westerlies and positive OLR anomalies over tropical Brazil gradually weaken and then reverse. The largest loadings throughout the evolution of the patterns contained in the first mode remain in the Tropics and subtropics. These results provide information on the combined relationship between atmospheric circulation and convection over the South American sector and on the evolution of patterns associated with 30–60 day (intraseasonal) oscillations. By projecting the combined fields of anomalous OLR and 250-mb zonal and meridional wind onto the individual patterns contained in the first rotated combined extended EOF mode, one obtains indices that should enhance real-time monitoring efforts and may lead to improved monthly forecasts for the South American sector.

1. Introduction

A better understanding of climate variations over South America on intraseasonal to interannual timescales requires a detailed study of the principal anomalous atmospheric circulation patterns dominating the region. Previous work has shown the importance of the El Niño–Southern Oscillation (ENSO) on interannual variability of rainfall over South America (e.g., Caviedes 1973; Hastenrath 1978; Streten 1983; Kousky et al. 1984; Ropelewski and Halpert 1987; Aceituno 1988; Kayano et al. 1988; Kousky and Ropelewski 1989). ENSO episodes feature abnormally warm sea surface temperatures throughout the equatorial central and eastern Pacific and anomalous convection in many regions of the Tropics and subtropics.

Excessive rainfall was observed in southern Brazil during the 1972–73 (Streten 1983) and the 1982–83 (Kousky et al. 1984; Kayano et al. 1988; Nobre and Oliveira 1986) warm (ENSO) episodes. Precipitation deficits in the eastern Amazon region and Northeast Brazil and excessive rainfall over coastal sections of Peru and Ecuador were observed during the 1982–83 ENSO episode (Nobre and Oliveira 1986; Kayano et al. 1988).

These precipitation anomalies have been attributed to large-scale changes in the global atmospheric circulation pattern associated with an anomalous eastward displacement of the Pacific Walker circulation that results in anomalous rising motion over the equatorial eastern Pacific and anomalous sinking motion

* Visiting UCAR scientist at the Climate Analysis Center, NOAA/NWS/NMC.

Corresponding author address: Dr. Vernon E. Kousky, Diagnostics Branch, Climate Analysis Center, NOAA/NWS/NMC, Washington, DC 20233.

over the tropical Atlantic (Kousky et al. 1984; Nobre and Oliveira 1986; Kayano et al. 1988). This abnormal Walker circulation is associated with enhanced convection over the abnormally warm waters of the eastern equatorial Pacific, while sinking motion farther east stabilizes the atmosphere over the tropical Atlantic and the eastern Amazon Basin.

Recent results by Rasmusson and Mo (1993), however, suggest an alternative explanation for the suppression of precipitation over northern South America. They suggest that an upper-tropospheric divergence anomaly zone, which extends from the enhanced convection in the central equatorial Pacific eastnortheastward across northern Mexico and then into the western Atlantic, is accompanied by a zone of compensating convergence on its equatorward flank. The corresponding sinking motion associated with this upper-level convergence, rather than a displaced Walker circulation cell, would then be responsible for the drier-than-normal conditions experienced in northern South America during warm episodes.

The excessive rainfall in southern Brazil during the fall and early winter months of 1983 has been shown to be related to a stronger-than-normal subtropical jet stream, a feature of warm episodes (Arkin 1982), accompanied by persistent upper-tropospheric blocking over the South American sector (Kousky et al. 1984; Kousky and Cavalcanti 1984). Under blocking conditions, the normal movement of transient systems is obstructed, so that Southern Hemisphere cold fronts stall over southern Brazil. During 1983, a quasi-stationary frontal zone served as a focus for frequent and intense periods of convection over southern Brazil.

Intraseasonal variability over South America may result from a variety of regional and large-scale phenomena. Slow-moving cold fronts and subtropical upper-tropospheric cyclonic vortices play an important role in modulating the precipitation in eastern Brazil mainly during the austral spring, summer, and fall seasons (Kousky 1979; Kousky and Gan 1981). Upper-tropospheric cyclonic vortices have been found on the eastern flank of the Bolivian anticyclone (Virji 1981) with a maximum frequency observed during the southern summer months (Kousky and Gan 1981). These systems can have a pronounced effect on the convection over eastern and northeastern Brazil (Kousky and Gan 1981). In addition, equatorward-moving southern cold fronts are very effective in organizing convection over eastern Brazil during the austral spring, summer, and fall seasons (Kousky 1979; Oliveira and Nobre 1986).

Observational evidence has been presented (Kousky and Gan 1981) illustrating some situations in which these two synoptic-scale systems are related to each other. The genesis of an upper-tropospheric cyclonic vortex depends upon the tropospheric circulation changes associated with southern midlatitude transient systems. Kousky and Gan proposed that the vortex formation is closely related to the development of a strong upstream upper-tropospheric ridge that intensifies because of low-level warm advection associated with an equatorward-moving cold front. These cold fronts are quite active and slow moving and may be major contributors to the South Atlantic convergence zone (SACZ), which is a prominent synoptic feature evident in satellite imagery during the spring and summer seasons (Casarin and Kousky 1986; Kousky and Cavalcanti 1988; Kousky 1988).

Variations in the position and intensity of the SACZ have been shown to be related to intraseasonal (30–60 day) oscillations in the South American sector (Casarin and Kousky 1986; Kousky and Cavalcanti 1988), which in turn are related to global-scale fluctuations in upper-tropospheric circulation and tropical convection (Weickmann et al. 1985; Casarin and Kousky 1986).

In this paper we describe the principal interannual and intraseasonal circulation modes over South America, obtained using combined empirical orthogonal function (EOF) analysis. The EOF analysis is performed on the same variables as those used in Kousky and Cavalcanti (1988). A major difference between Kousky and Cavalcanti (1988) and this paper concerns the filtering performed prior to computing the EOFs. Data filtering is adopted to make a clear distinction between the patterns related to interannual climatic fluctuations and those linked to shorter-timescale intraseasonal oscillations. In addition, we make use of extended EOF analysis to determine the evolution of anomaly patterns associated with intraseasonal oscillations.

2. Data and analysis procedure

The dataset used consists of five-day (pentad) nonoverlapping means of the 250-mb zonal and meridional wind components taken from the analyses of the National Meteorological Center (NMC). In addition, pentad means of outgoing longwave radiation (OLR), observed from the National Oceanic and Atmospheric Administration's (NOAA) polar-orbiting satellites, are used to indicate variations in deep convection within the Tropics. Both datasets are available at the Climate Analysis Center, Washington, D.C. The circulation data, used extensively in previous studies on interannual and intraseasonal variability (e.g., Arkin 1982; Weickmann 1983; Weickmann et al. 1985; Rasmusson and Arkin 1985), are adequate for describing the large-scale features associated with the Southern Oscillation and with intraseasonal (30–60 day) oscillations. The OLR data provide information on the distribution and intensity of tropical convection (Leibmann and Hartmann 1982; Rasmusson and Arkin 1985). Studies (Chang and Kousky 1987; Chelliah and Arkin 1992) have shown, however, that differences in equator crossing times among the various polar-orbiting sat-

TABLE 1. Polar-orbiting satellites and equator crossing times.

	Equator crossing time (LST)	Period
TIROS-N	1500	Jan 1979–Jan 1980
NOAA-6	1930	Feb 1980–Aug 1981
NOAA-7	1430	Sep 1981–Feb 1985
NOAA-9	1420	Mar 1985–Nov 1988
NOAA-11	1340	Nov 1988–Aug 1992

ellites (Table 1), used in determining the OLR, produce a large-scale interannual pattern of OLR anomalies that reflects the different sampling times of the diurnal cycle. To minimize this effect, we removed the mean OLR anomaly patterns from the data for periods corresponding to when the *TIROS-N* and *NOAA-6, -7, -9,* and *-11* satellites were operational (Table 1).

The period of analysis used in determining the principal modes is January 1979 through December 1991 (totaling 949 pentads). The data have a resolution of 2.5 degrees in latitude and longitude. The area considered in this study is limited to the region from 20°N to 50°S and 10°W to 100°W, which covers all except extreme southern South America. The reader is cautioned that the physical interpretation of OLR at latitudes higher than 30° is difficult, especially during the cold season, as low values of OLR can result from either clouds or surface cooling in continental regions.

The variables in the area of interest are selected for every other grid point, thus reducing the resolution to 5 degrees in latitude and longitude. This is more than adequate to describe the principal large-scale patterns that affect the region. Anomalies for each variable are calculated by removing the smoothed 1979–1988 pentad means. An OLR climatology for a shorter period, and its method of computation, was described by Kousky (1988). The same method was applied in developing the base-period means for the OLR and 250-mb wind components used in this study.

The use of pentad data results in effectively removing high-frequency transients associated with individual weather events. Additional temporal filtering on all variables is done by applying a Lanczos filter. For a detailed description of this filter, see Duchon (1979). The weights for this filter are computed from

$$w_k = \left(\frac{\sin 2\pi f_{c1}k}{\pi k} - \frac{\sin 2\pi f_{c2}k}{\pi k}\right)\frac{\sin \pi k/n}{\pi k/n}, \quad (1)$$

where n is the number of weights, $k = -n, \cdots, n$, and f_{c1} and f_{c2} are the cutoff frequencies. For the case of a low-pass filter, f_{c2} is set to zero and f_{c1} is set to 0.0275 pentads^{-1}, which corresponds to a filter response of 0.5 at 180 days (36 pentads). Our choice of $n = 48$ was determined based on our desire to use as few weights as possible and still have a rather sharp filter (the sharpness of the filter increases as the number of weights, n, increases). For our study of intraseasonal variations, we use a bandpass filter where the weights are computed from (1) using $f_{c1} = 0.2$ pentads^{-1} and $f_{c2} = 0.0575$ pentads^{-1}. The frequency response functions

$$R(f) = w_0 + 2\sum_{k=1}^{n} w_k \cos 2\pi f k \quad (2)$$

for the low-pass and bandpass filters are shown in Fig. 1. The low-pass filtered time series, with all high-frequency variations removed, are used to determine the principal modes of interannual (IA) variability. Similarly, the bandpass-filtered time series are used to determine the modes of intraseasonal (IS) variability.

Combined unrotated and rotated EOFs, using the varimax method, are computed based on an array of correlations in which all three anomaly fields (OLR and 250-mb zonal and meridional wind components) are included for the study area. The resulting EOF patterns for anomalous OLR are, therefore, physically consistent with the 250-mb circulation anomalies.

The choice of the number of eigenmodes to rotate is based on a plot of the fractional explained variance versus unrotated mode number (O'Lenic and Livezey 1988). The curve in this plot contains sections where the slope is relatively small (giving the appearance of shelves) with adjacent modes explaining similar fractions of the total variance. The number of modes used in the rotated analysis is determined by taking all modes up to and including the last mode in a shelf region. The number of eigenmodes to rotate is not the same for all cases, so the number used for each case will be specified when discussing the results. For more details concerning the selection criteria in a rotated EOF analysis, the reader is referred to O'Lenic and Livezey (1988).

The principal component time series (amplitude time series of the EOF modes) are analyzed to investigate the seasonal and interannual variability of each

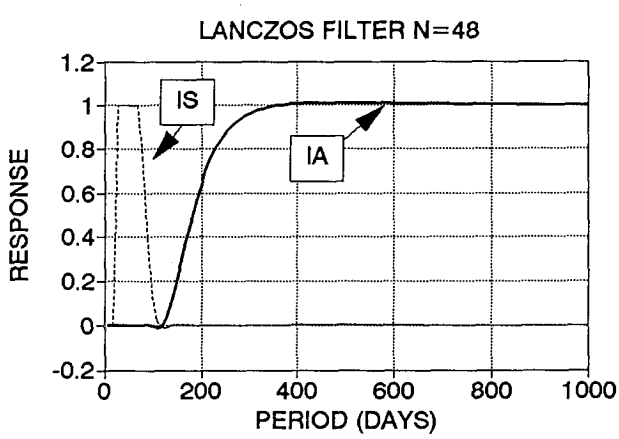

FIG. 1. Lanczos filter response for the IA (heavy solid line) and IS bandpass (dashed line) filters.

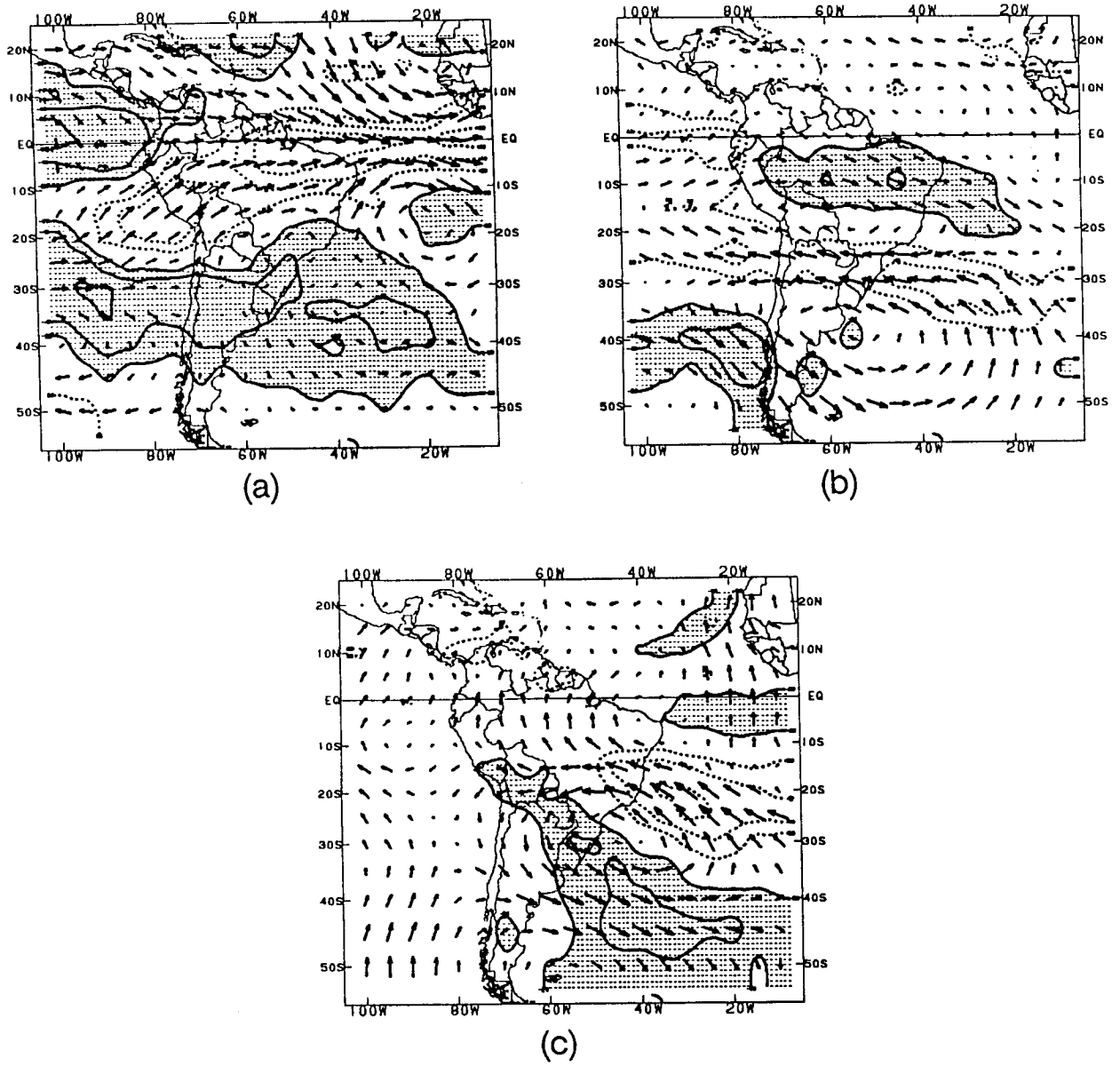

FIG. 2. The first three combined (OLR and 250-mb vector wind) unrotated IA patterns (a–c, respectively), computed for the period 1979–91. The 250-mb circulation loadings are indicated by vectors. The OLR loadings are contoured with negative (positive) values indicated by solid (dashed) lines. The zero line has been omitted. Negative values are shaded.

pattern. The time evolution of the spatial patterns in the IS band is investigated using extended EOF (EEOF) analysis (Weare and Nasstrom 1982). EEOF analysis uses not only the fields at time = t, but also the fields at other times—for example, $t + \Delta t$, $t + 2\Delta t$. Consequently, the resulting modes describe a temporal evolution. The EEOF analysis was performed using the combined fields of anomalous OLR and 250-mb zonal and meridional wind components. This resulted in a substantial increase in the size of the correlation matrix, which forced us to reduce the resolution of the data to 10° in latitude and longitude. To maximize local variance within the domain, we rotated the EEOF modes (Lau and Lau 1990) using the varimax method. The loading patterns for the rotated EEOF analysis are interpolated to a 5° by 5° grid for display purposes.

3. Interannual modes

In this section, we present the patterns for the first three unrotated IA modes. The corresponding patterns for the first three rotated IA modes (not shown) are quite similar. The first unrotated IA mode has its maximum circulation and OLR loadings in the Tropics

(Fig. 2a) and explains 13.5% of the IA variance. The maximum loading for anomalous OLR of 0.8 over the mouth of the Amazon indicates that this mode explains 64% of the IA variance in that region. The maximum loading for u anomalies is 0.9 along and south of the equator in the longitude band 20°–35°W, indicating that approximately 80% of the IA variance of the 250-mb zonal wind is explained by the first mode in that region. For positive (negative) amplitudes of this mode, upper-tropospheric westerly (easterly) anomalies and positive (negative) OLR anomalies dominate the region between 10°N and 10°S from western Brazil eastward to the west coast of Africa. A cyclonic (anticyclonic) anomaly couplet is found straddling the equator in the tropical Atlantic. The plot of the time series of the principal components (amplitudes) for this mode (Fig. 3a, thin line) shows large positive values during 1982–83 and 1986–87, and large negative values during 1988–89. These periods coincide with the major extremes in the Southern Oscillation during our period of study.

To compare the amplitude time series with the Southern Oscillation, we computed a pentad Southern Oscillation index (SOI) based on gridded sea level pressure analyses. The grid points nearest in location to Tahiti and Darwin were used to compute the SOI, which was calculated using the same procedure as that described by Chelliah (1990). The pentad values of the SOI were smoothed using the low-pass Lanczos filter in the same manner as the data were filtered prior to performing the combined EOF analysis. For comparison purposes, the filtered pentad SOI is also shown in Fig. 3a (heavy line). The simultaneous correlation between the two time series in Fig. 3a is −0.77.

The first mode contains many atmospheric features previously found to be associated with extremes in the Southern Oscillation. For positive amplitudes of the first mode (negative extremes of the Southern Oscillation, or warm episodes), positive OLR anomalies extend from the Amazon Basin eastward across Northeast Brazil and the equatorial Atlantic. Negative OLR anomalies are found over the eastern equatorial Pacific, over the subtropical eastern South Pacific, and over central South America. The relationship between drier-than-normal conditions over Northeast Brazil and warm (ENSO) episodes has been extensively studied in previous works (e.g., Caviedes 1973; Hastenrath and Heller 1977; Kousky et al. 1984; Ropelewski and Halpert 1987; Aceituno 1988). It is apparent from Fig. 2a that, during warm episodes, drier-than-normal conditions also extend southwestward from the mouth of the Amazon across most of Bolivia and southern Peru. A similar pattern has been noted by Aceituno (1988). The pattern of anomalously strong upper-tropospheric westerlies over the equatorial Atlantic during negative extremes of the Southern Oscillation is a feature generally observed during Pacific warm episodes (Arkin 1982; Mo and Kousky 1993). The opposite features were observed during the 1988–89 Pacific cold episode (high SOI) (Kousky and Ropelewski 1989; Arkin 1989; Mo 1989).

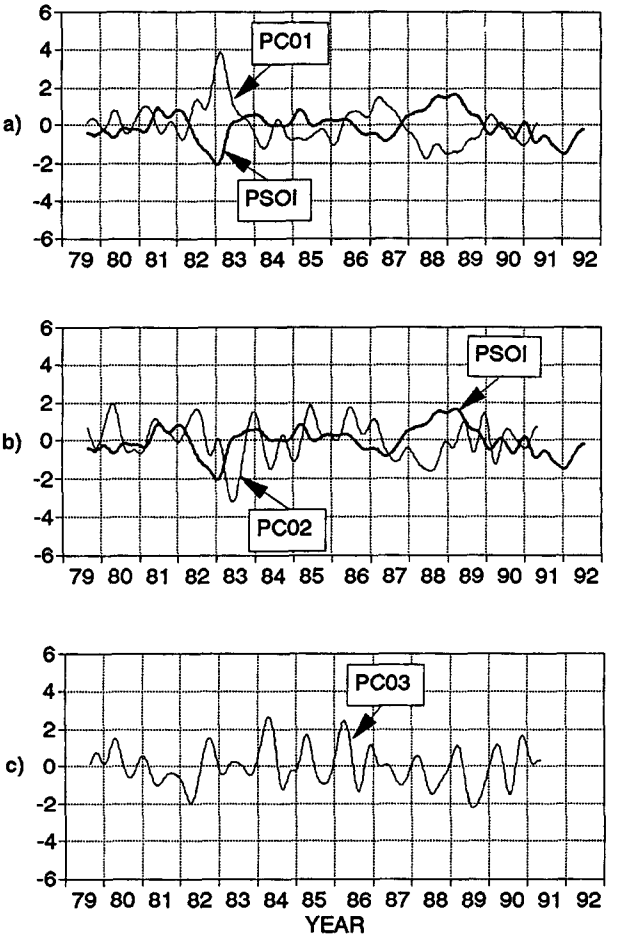

FIG. 3. Amplitude time series (thin lines) for the first three unrotated IA modes shown in Fig. 2. For comparison, the time series of the pentad Southern Oscillation index (PSOI) is shown in (a) and (b).

The second unrotated IA mode, which explains 8.4% of the variance, has its largest loadings in the subtropics and midlatitudes of the Southern Hemisphere (Fig. 2b). For positive (negative) amplitudes of this mode, upper-tropospheric anticyclonic (cyclonic) circulation anomalies dominate the region of central Argentina and the neighboring western Atlantic, and positive (negative) OLR anomalies extend from the eastern Pacific, near 25°S, eastward across northern Argentina and southern Brazil to the western Atlantic. Negative (positive) OLR anomalies are also found in an east–west band across tropical Brazil, with a cyclonic (anticyclonic) circulation anomaly to the south. This mode describes interannual variations in the intensity of the subtropical jet stream in the South American sector.

The amplitude time series for this mode, shown in Fig. 3b (thin line), shows the tendency for extreme amplitudes to occur during the southern winter season. It is also evident that negative (positive) extremes tend to occur during and after negative (positive) extremes of the SOI (Fig. 3b, heavy line). The maximum lagged correlation between the two series is 0.34 for the SOI leading the amplitude time series by 30 pentads. This rather weak relationship signifies that IA variations in the intensity of the subtropical westerlies over South America are only partially related to the Southern Oscillation.

Features described in the second IA mode are consistent with those found in previous studies of circulation anomalies related to ENSO. Stronger-than-normal subtropical jet streams in both hemispheres have been observed in the Pacific sector during warm episodes (Arkin 1982) and have been related to enhanced rainfall over subtropical regions of North and South America (e.g., Kousky and Ropelewski 1989). The enhanced jet streams form on the poleward flanks of anomalous upper-tropospheric anticyclonic circulation centers found at low latitudes in the central Pacific in association with enhanced equatorial convection in that region. The enhanced westerlies also form part of a wave train of anomalous circulation features that emanate from the central Pacific toward higher latitudes of the winter hemisphere (Horel and Wallace 1981; Karoly 1989). For negative amplitudes of the second IA mode (warm episodes), a cyclonic circulation center is observed near the coast of Argentina (Fig. 2b), which is consistent with the Southern Hemisphere wave train described by Karoly (1989).

For positive amplitudes (cold episodes), this mode describes a pattern of weaker-than-normal subtropical westerlies and drier-than-normal conditions over northern Argentina and southern Brazil. These precipitation anomalies are consistent with those found associated with periods of high SOI (Ropelewski and Halpert 1989). The opposite pattern, however, was not found during the winter for the composite of several warm episodes (Ropelewski and Halpert 1987). Above-normal cool season (fall and early winter) rainfall was observed over southern Brazil during the warm episodes of 1972–73, 1976–77, and 1982–83, but the pattern varied substantially from episode to episode (Kousky et al. 1984). This spatial variability of winter precipitation anomalies among warm episodes may be the reason that a consistent pattern of winter precipitation anomalies was not found in the objective analysis of Ropelewski and Halpert (1987).

The third unrotated IA mode, shown in Fig. 2c, explains 7.4% of the variance. In contrast to the first two modes, this mode does not show any significant relationship to the Southern Oscillation. For positive (negative) amplitudes of this mode, an anomalous anticyclonic (cyclonic) circulation center is found near the coast of southern Brazil, with positive (negative) OLR anomalies to the northeast of the center and negative (positive) OLR anomalies to the southwest of the center. There is a pronounced annual cycle in the amplitude time series for this mode during 1984–86 and late 1987–early 1990 (Fig. 3c), with positive amplitudes occurring during the early part of each year and negative amplitudes occurring during late winter or early spring (August–October). During the southern summer, this pattern appears to be related to anomalous shifts in the position of the South Atlantic convergence zone.

To address the question of the importance of the first three modes in the raw unfiltered data, we projected the original data onto each of the first three modes and then filtered the projected time series with the low-pass Lanczos filter. These time series are shown in Fig. 4. The smoothed projected time series for each mode show the same characteristics as the amplitude time series (Fig. 3). The low-frequency signal appears to be strongest in the first mode (Fig. 4a), somewhat evident in the second mode (Fig. 4b), especially during 1982–83, and quite weak in the

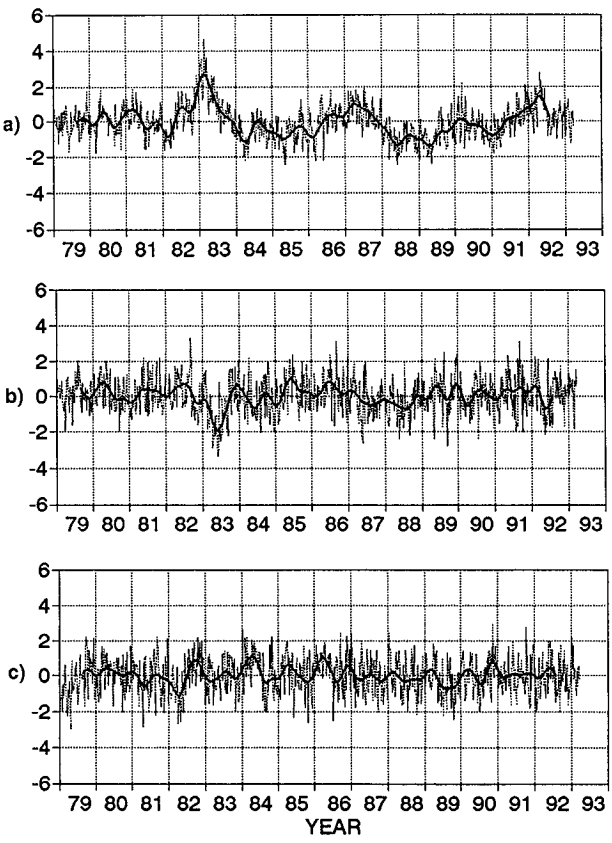

FIG. 4. Smoothed (low-pass Lanczos filtered, heavy line) and unsmoothed (dashed line) time series obtained by projecting the original data onto the first (a), second (b), and third (c) unrotated IA modes. Data are normalized by the standard deviation for the period 1979–88.

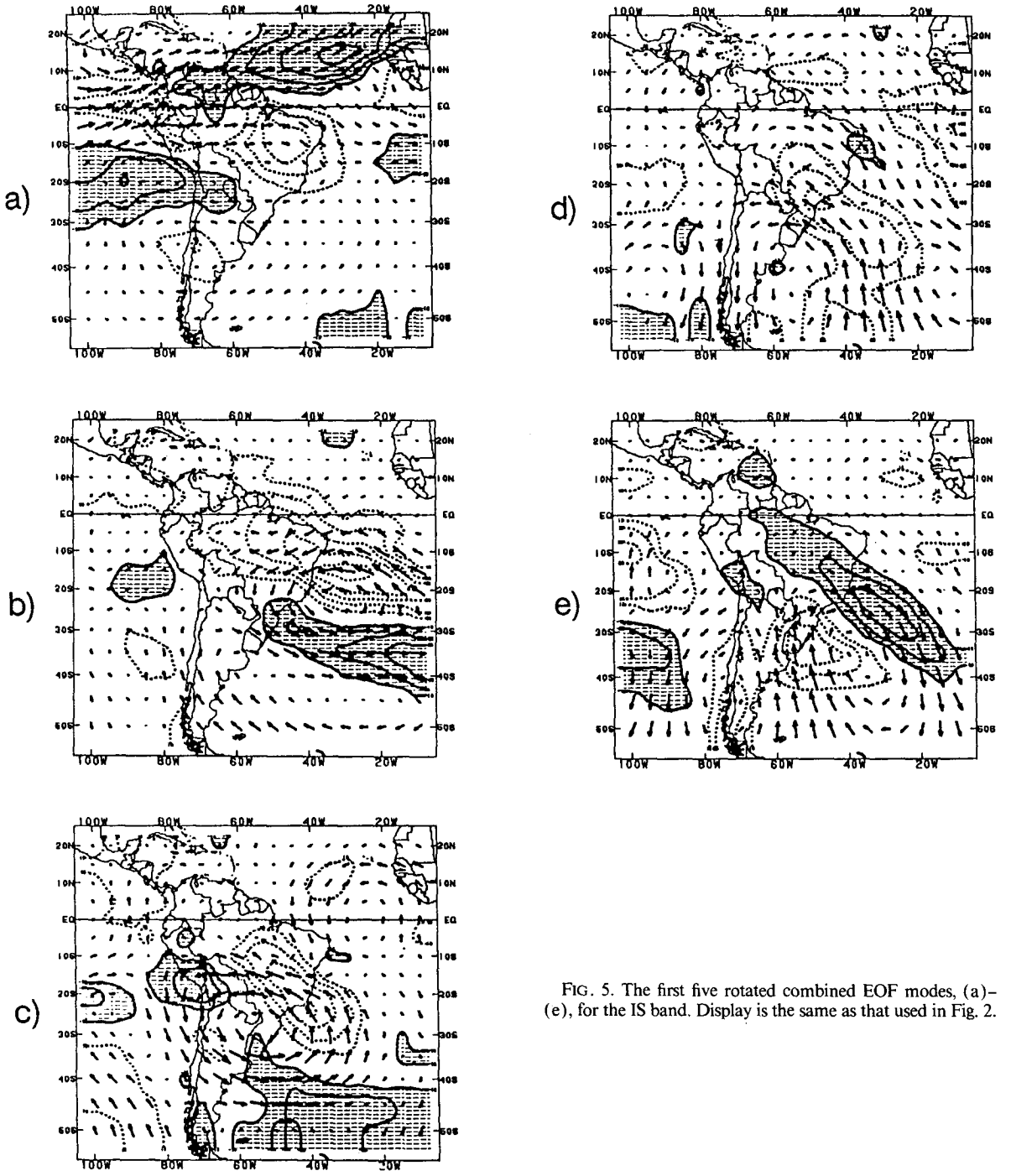

FIG. 5. The first five rotated combined EOF modes, (a)–(e), for the IS band. Display is the same as that used in Fig. 2.

third mode (Fig. 4c). To quantify this, we computed the ratio between the low-frequency variance and the total variance for each of the first three modes. For the first mode, low-frequency variability accounts for 60% of the total variance, while for the second and third modes it accounts for 23% and 18% of the total variance, respectively.

The first two IA modes contain many features previously identified as related to extremes in the Southern Oscillation. Unlike many previous studies, our patterns are not dependent on a sparse network of surface observing stations. Since our patterns agree with previous studies for the data-rich areas, it is likely that our patterns are realistic over the more data-sparse regions,

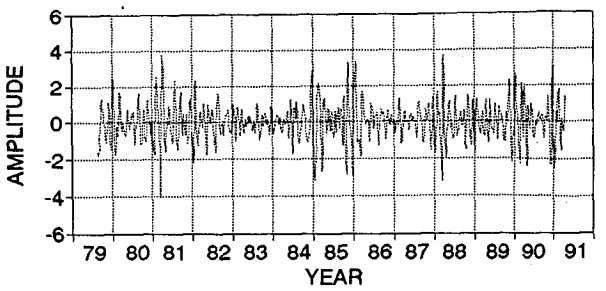

FIG. 6. The amplitude time series for the first rotated combined EOF mode in the IS band.

such as over the Amazon Basin and the Atlantic and Pacific Oceans.

4. Intraseasonal modes

a. Combined EOF analysis

Using the criteria suggested by North et al. (1982), we determined that the first and second combined unrotated IS modes are degenerate. Therefore, we performed a series of rotated combined EOF (RCEOF) analyses using a varying number of unrotated modes (15 to 41). The first rotated mode remained the same in each analysis. The higher modes maintained similar patterns, but their order changed depending on the number of unrotated modes used in the rotated analysis. The first five rotated IS modes, using 15 unrotated modes, are shown in Fig. 5. These explain 24% of the total IS variance. The first mode (Fig. 5a) explains 5.6% of the variance and has its largest loadings in the Tropics. For positive (negative) amplitudes of this mode, anomalous upper-tropospheric westerly (easterly) flow dominates the Tropics throughout the region. Positive (negative) OLR anomalies are observed over northeastern South America and over the eastern equatorial Pacific. Negative (positive) OLR anomalies are found over the subtropical North Atlantic. A similar pattern of OLR anomalies has been observed over the South American sector associated with the 30–60 day (Madden–Julian) oscillation (Weickmann et al. 1985).

The first rotated IS mode is most active during the Southern Hemisphere summer season (Fig. 6). To illustrate this seasonality, we computed the variance of the amplitude for this mode for overlapping 11-pentad periods for the entire record (Fig. 7). The variance is clearly greatest during the southern summer and shows considerable IA variability. This mode was most active during the summers of 1980/81, 1984/85, 1985/86, 1987/88, 1989/90, and 1990/91, and least active during the summers of 1982/83, 1983/84, 1986/87, and 1988/89. A comparison of Fig. 7 with the SOI (Fig. 3, heavy line) reveals that extreme (neutral) years in the Southern Oscillation are characterized by weaker (stronger) variability of this mode.

The second rotated IS mode (Fig. 5b) has its greatest loadings in the western subtropical Atlantic. For positive (negative) amplitudes of this mode, anomalous anticyclonic (cyclonic) upper-tropospheric circulation is found in the western Atlantic near the Southeast Brazilian coast. Positive (negative) OLR anomalies are found over northeastern South America and the neighboring western Atlantic, and negative (positive) OLR anomalies extend from southern Brazil eastsoutheastward across the lower midlatitudes of the Atlantic. The amplitude time series and variance time series (not shown) do not indicate any significant seasonality or IA variability in the activity of this mode.

The third rotated IS mode (Fig. 5c) has its greatest loadings over subtropical South America. Similar to the second IS mode, this mode does not show any significant seasonality in its activity. The fourth and fifth rotated IS modes (Figs. 5d and 5e) have their maximum loadings in the subtropics and midlatitudes. These modes also do not display any significant seasonality.

Modes 2–5 have their greatest loadings in the low- to midlatitudes of the Southern Hemisphere. Thus, it is likely that they are associated with persistent anomalous features such as blocking or slowly evolving planetary waves. In addition, each of these modes involves large OLR loadings over eastern South America, which further suggests that these modes are also associated with variations in intensity and shifts in the position of the SACZ.

b. Extended EOF analysis

The RCEOF analysis, described in the preceding section, identifies physically consistent IS patterns but does not provide information concerning the evolution of the individual modes. This information would be useful for real-time monitoring and prediction efforts. To determine the evolution of the IS modes, we performed a rotated combined extended EOF (RCEEOF) analysis on the bandpass-filtered data. Once again we made a series of analyses using a varying number of unrotated modes. Using a greater number of unrotated modes resulted in smoother patterns. In this section

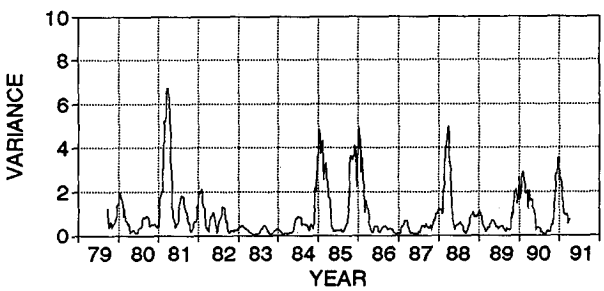

FIG. 7. The variance of the time series shown in Fig. 6, computed for overlapping 11-pentad periods.

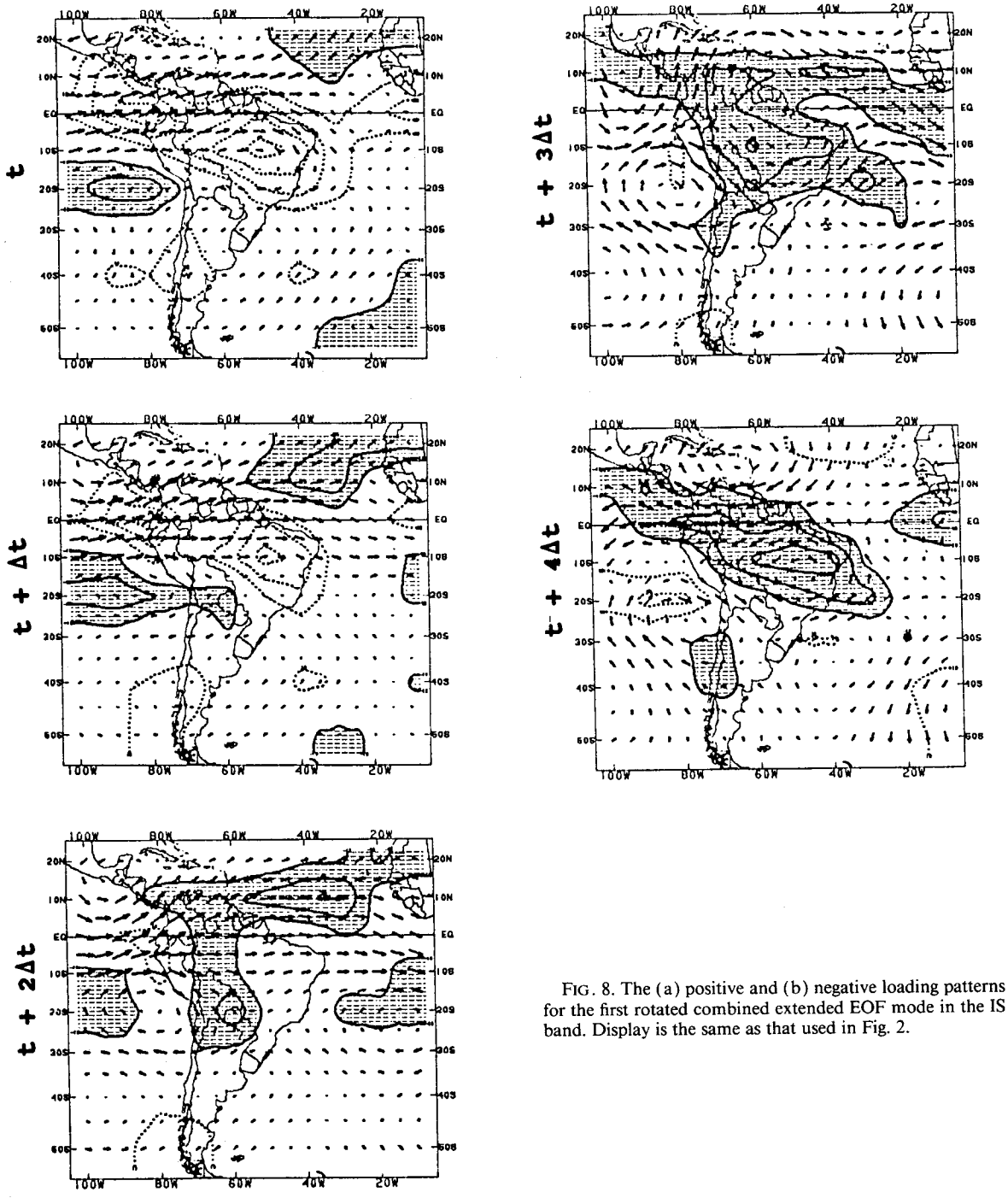

FIG. 8. The (a) positive and (b) negative loading patterns for the first rotated combined extended EOF mode in the IS band. Display is the same as that used in Fig. 2.

we discuss the case where 46 unrotated modes (explaining 68% of the total IS variance) were used in the rotated extended EOF analysis.

The extended EOF analysis technique emphasizes the cyclical behavior in the evolution of anomaly patterns. Therefore, for each evolving pattern, the analysis results in two modes that describe a similar evolution, but with the patterns for time = t being 90 degrees out of phase. The first and second RCEEOF modes describe an evolution of the first RCEOF mode (Fig. 5a). Together they explain 6.5% of the intraseasonal variance. To obtain a complete cycle, we show the patterns for the positive and negative loadings of the first mode (Figs. 8a and 8b, respectively). The time interval (Δt) used in the analysis is one pentad. Thus, the period of the oscillation represented in Fig. 8 is approximately 40–45 days.

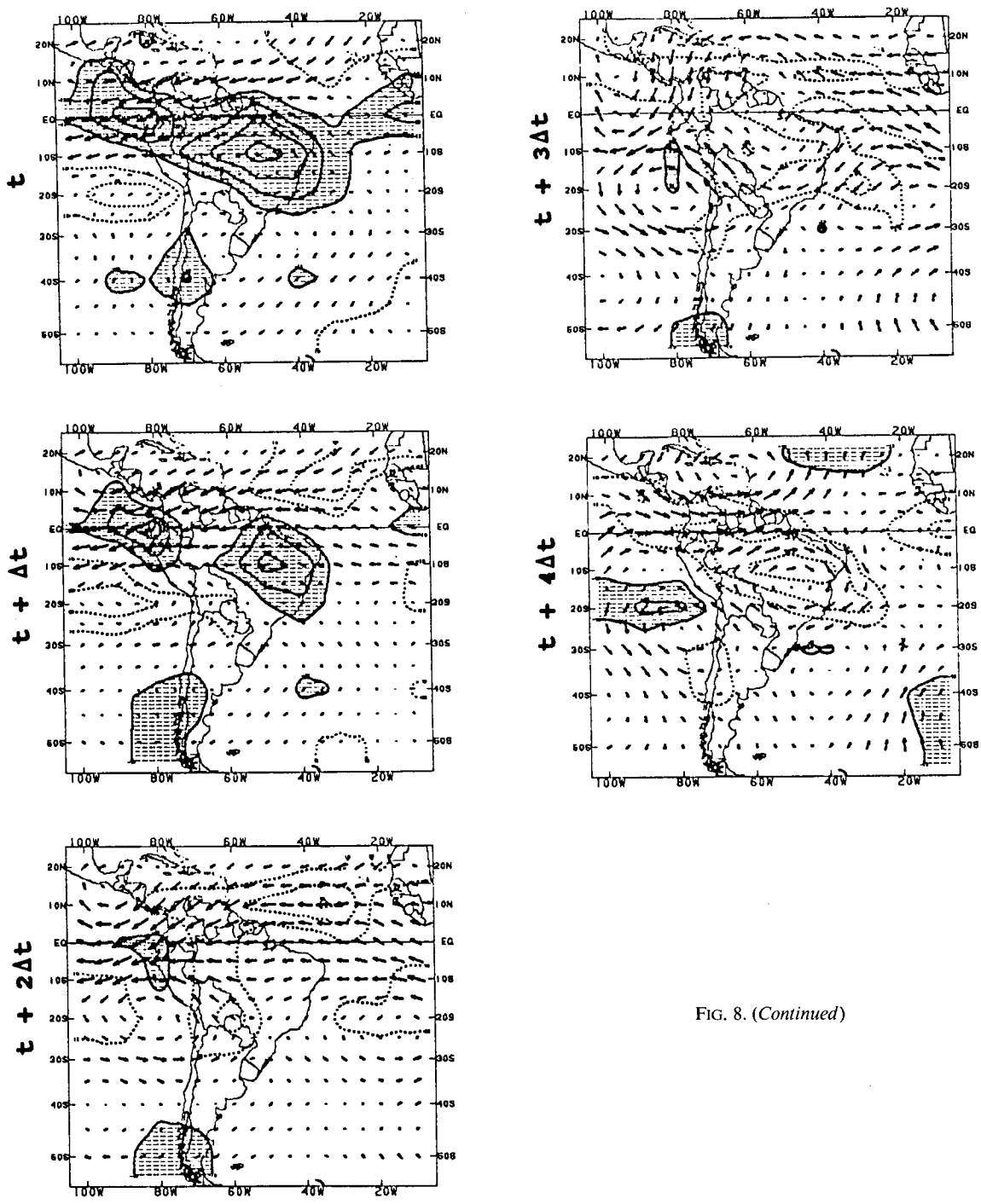

FIG. 8. (*Continued*)

The pattern at time t in Fig. 8a is similar to that of the first RCEOF mode (Fig. 5a). In the sequence shown in Fig. 8, the pattern of anomalous equatorial westerlies and positive OLR anomalies over tropical Brazil gradually weakens and then reverses. The largest loadings throughout the evolution of these patterns remain in the Tropics and subtropics. As convection becomes enhanced over the Amazon Basin (time $t + 2\Delta t$ to $t + 4\Delta t$, Fig. 8a, and continuing on to time t of Fig. 8b), an anomalous anticyclonic circulation couplet develops near 60°W, with centers over central Brazil and over the eastern Caribbean Sea. Accompanying this evolution, the upper-tropospheric westerly anomalies weaken and are replaced by easterly anomalies. The northwest–southeast orientation of the negative OLR loadings over tropical Brazil, shown at times $t + 4\Delta t$

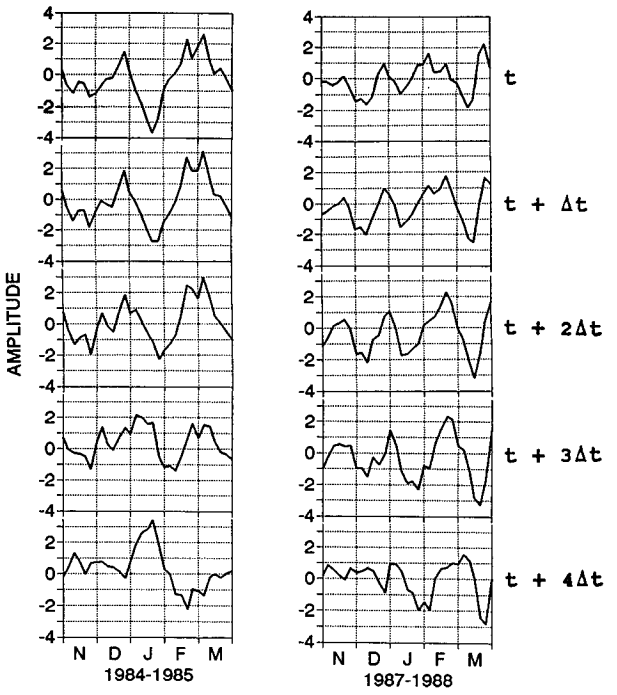

FIG. 9. Time series of the amplitudes of the patterns contained in the first rotated combined extended EOF mode, for November–March 1984–85 and 1987–88. Amplitudes are obtained by projecting the unfiltered anomaly fields onto the individual loading patterns at times t to $t + 4\Delta t$.

(Figs. 8a and 8b), suggests a modulation in the position and intensity of the SACZ.

The relationship between upper-tropospheric flow anomalies and OLR anomalies, which is shown in Fig. 8, is consistent with previous theoretical studies on atmospheric circulation related to anomalous tropical heating (Webster 1972; Gill 1980) and with observational studies describing the relationship between upper-tropospheric circulation changes and variations in convection over South America (Kousky 1985). Similar variations in the position of the SACZ, related to intraseasonal variations in the South American sector, have been noted previously by Casarin and Kousky (1986).

By projecting the combined fields of anomalous OLR and 250-mb zonal and meridional wind onto the individual patterns contained in the first RCEEOF mode, we obtain five time series. These can be used to assess the amplitude and period of the intraseasonal oscillation in the South American sector. Examples of these time series are shown in Fig. 9 for the months of November through March during 1984–85 and 1987–88. The evolution of this mode can be determined by noting the temporal shifts of the maxima and minima among the five time series. For the 1984–85 period, the evolution was more gradual (longer period oscillation) than that observed during 1987–88. Also, the amplitude range of the patterns for times t and $t + \Delta t$ was greater in 1984–85. Since these patterns contain the greatest loadings for OLR in the evolution of this mode, one can conclude that the variability in tropical convection associated with the intraseasonal oscillations was greater during 1984–85. Projecting the current anomaly fields onto the loading patterns for this mode should enhance real-time monitoring efforts and may lead to improved monthly forecasts for the South American sector.

None of the other pairs of modes resulting from the RCEEOF analysis produced patterns that evolved in a similar manner as the first and second modes. Those higher modes are probably related to more randomly occurring persistent anomalies, such as blocking episodes and variations in the zonal index.

5. Summary and conclusions

An EOF analysis for the South American sector was performed using filtered data that allowed interannual and intraseasonal modes to be studied independently. The first interannual mode contains many atmospheric features related to extremes in the Southern Oscillation, such as 1) positive (negative) OLR anomalies over the Amazon Basin, Northeast Brazil, and the equatorial Atlantic, and 2) negative (positive) OLR anomalies over the equatorial and subtropical eastern Pacific, and over central South America during warm (cold) episodes. Features of the second IA mode describe subtropical and lower-midlatitude anomaly patterns that are, in part, associated with ENSO. During the latter stages of warm episodes, this mode is associated with stronger-than-normal subtropical westerlies and with enhanced rainfall over central South America. These enhanced westerlies, and the anomalous cyclonic circulation center on their poleward flank, are part of a wave train of anomalous circulation features that emanates from the central Pacific toward higher latitudes in the Southern Hemisphere (Karoly 1989).

The first intraseasonal mode has its greatest loadings in the Tropics and is most active during the southern summer season. For positive (negative) amplitudes of this mode, anomalous upper-tropospheric westerly (easterly) flow dominates the Tropics throughout the region, and positive (negative) OLR anomalies are observed over northeastern South America and over the eastern equatorial Pacific. A similar pattern of OLR anomalies over the South American sector has been found in association with the 30–60 day (Madden–Julian) oscillation (Weickmann et al. 1985).

The RCEOF analysis identified physically consistent patterns of atmospheric circulation and OLR but did not provide information concerning the evolution of these patterns. This is most important in the study of intraseasonal variations. To address this issue, an extended combined EOF analysis was performed to study the evolution of intraseasonal oscillations in the South American sector. The first RCEEOF mode describes a

sequence of patterns in which anomalous equatorial westerlies and positive OLR anomalies over tropical Brazil gradually weaken and then reverse. The largest loadings throughout the evolution of these patterns remain in the Tropics and subtropics. These results are consistent with previous studies on intraseasonal variations and provide additional information on the combined relationship between atmospheric circulation and convection over the South American sector. By projecting the combined fields of anomalous OLR and 250-mb zonal and meridional wind onto the individual patterns contained in the first RCEEOF mode, one obtains indices that should enhance real-time monitoring efforts and may lead to improved monthly forecasts for the South American sector.

Acknowledgments. The authors thank Kingtse Mo and Ed O'Lenic for reviewing an earlier version of this paper, and John Kopman for his help in preparing the figures. The comments and suggestions of the anonymous official reviewers, which led to significant changes in the final version of this paper, are greatly appreciated.

REFERENCES

Aceituno, P., 1988: On the functioning of the Southern Oscillation in the South American sector. *Mon. Wea. Rev.*, **116,** 505–525.

Arkin, P. A., 1982: The relationship between interannual variability in the 200-mb tropical wind field and the Southern Oscillation. *Mon. Wea. Rev.*, **110,** 1393–1404.

——, 1989: The global climate for December 1988–February 1989: Cold episode in the tropical Pacific continues. *J. Climate,* **2,** 737–757.

Casarin, D. P., and V. E. Kousky, 1986: Rainfall anomalies in southern Brazil and related atmospheric circulation features. *Rev. Bras. Meteor.*, **1,** 83–90 (in Portuguese).

Caviedes, C. N., 1973: Secas and El Niño: Two simultaneous climatical hazards in South America. *Proc. Assoc. Amer. Geogr.*, **5,** 44–49.

Chang, F. C., and V. E. Kousky, 1987: An observational study of interaction between large scale tropical cumulus convection and the equatorial circulation anomalies. *Proc. 12th Annual Climate Diagnostics Workshop,* Salt Lake City, Climate Analysis Center and Department of Meteorology, University of Utah, 256–265.

Chelliah, M., 1990: The global climate for June–August 1989: A season of near-normal conditions in the tropical Pacific. *J. Climate,* **3,** 138–162.

——, and P. A. Arkin, 1992: Large-scale interannual variability of monthly outgoing longwave radiation anomalies over the global tropics. *J. Climate,* **5,** 371–389.

Duchon, C. E., 1979: Lanczos filtering in one and two dimensions. *J. Appl. Meteor.*, **18,** 1016–1022.

Gill, A. E., 1980: Some simple solutions for heat-induced tropical circulation. *Quart. J. Roy. Meteor. Soc.*, **106,** 447–462.

Hastenrath, S., 1978: On modes of tropical circulation and climate anomalies. *J. Atmos. Sci.*, **35,** 2222–2231.

——, and L. Heller, 1977: Dynamics of climatic hazards in Northeast Brazil. *Quart. J. Roy. Meteor. Soc.*, **103,** 77–92.

Horel, J. D., and J. M. Wallace, 1981: Planetary-scale atmospheric phenomena associated with the Southern Oscillation. *Mon. Wea. Rev.*, **109,** 813–829.

Karoly, D. J., 1989: Southern Hemisphere circulation features associated with El Niño–Southern Oscillation events. *J. Climate,* **2,** 1239–1252.

Kayano, M. T., V. B. Rao, and A. D. Moura, 1988: Tropical circulation and associated rainfall anomalies during 1983–1984. *J. Climatol.*, **8,** 477–488.

Kousky, V. E., 1979: Frontal influences on northeast Brazil. *Mon. Wea. Rev.*, **107,** 1140–1153.

——, 1985: Atmospheric circulation changes associated with rainfall anomalies over tropical Brazil. *Mon. Wea. Rev.*, **113,** 1951–1957.

——, 1988: Pentad outgoing long wave radiation climatology for the South American sector. *Rev. Bras. Meteor.*, **3,** 217–231.

——, and M. A. Gan, 1981: Upper tropospheric cyclonic vortices in the tropical South Atlantic. *Tellus,* **33,** 538–551.

——, M. T. Kayano, and I. F. A. Cavalcanti, 1984: A review of the Southern Oscillation: Oceanic–atmospheric circulation changes and related rainfall anomalies. *Tellus,* **36A,** 490–502.

——, and I. F. A. Cavalcanti, 1984: El Niño–Southern Oscillation events: Characteristics, evolution and precipitation anomalies. *Ciênc. Cult.*, **36,** 1888–1899.

——, and I. F. A. Cavalcanti, 1988: Precipitation and atmospheric circulation anomaly patterns in the South American sector. *Rev. Bras. Meteor.*, **3,** 199–206.

——, and C. F. Ropelewski, 1989: Extremes in the Southern Oscillation and their relationship to precipitation anomalies with emphasis on the South American region. *Rev. Bras. Meteor.*, **4,** 351–363.

Lau, K.-H., and N.-C. Lau, 1990: Observed structure and propagation of tropical summertime synoptic-scale disturbances. *Mon. Wea. Rev.*, **118,** 1888–1913.

Leibmann, B., and D. L. Hartmann, 1982: Interannual variations of outgoing IR associated with tropical circulation changes during 1974–78. *J. Atmos. Sci.*, **39,** 1153–1162.

Mo, K. C., 1989: The global climate for March–May 1989: Cold episode in the tropical Pacific decays. *J. Climate,* **2,** 1107–1129.

——, and V. E. Kousky, 1993: Further analysis of the relationship between circulation anomaly patterns and tropical convection. *J. Geophys. Res.*, **98,** 5103–5113.

Nobre, C. A., and A. S. Oliveira, 1986: Precipitation and circulation anomalies in South America and the 1982–83 El Niño/Southern Oscillation episode. *Extended Abstracts, Second Int. Conf. on Southern Hemisphere Meteorology,* Wellington, New Zealand, Amer. Meteor. Soc., 442–445.

North, G. R., T. L. Bell, R. F. Cahalan, and F. J. Moeng, 1982: Sampling errors in the estimation of empirical orthogonal functions. *Mon. Wea. Rev.*, **110,** 699–706.

O'Lenic, E. A., and R. L. Livezey, 1988: Practical considerations in the use of rotated principal component analysis (RPCA) in diagnostic studies of upper-air height fields. *Mon. Wea. Rev.*, **106,** 1682–1689.

Oliveira, A. S., and C. A. Nobre, 1986: Interactions between frontal systems in South America and tropical convection over the Amazon. *Extended Abstracts, Second Int. Conf. on Southern Hemisphere Meteorology,* Wellington, New Zealand, Amer. Meteor. Soc., 56–59.

Rasmusson, E. M., and P. A. Arkin, 1985: Interannual climate variability associated with the El Niño/Southern Oscillation. *Coupled Ocean–Atmosphere Models,* J. C. J. Nihoul, Ed., Elsevier, 289–302.

——, and K. Mo, 1993: Linkages between 200-mb tropical and extratropical circulation anomalies during the 1986–1989 ENSO cycle. *J. Climate,* **4,** 595–616.

Ropelewski, C. F., and M. S. Halpert, 1987: Global and regional scale precipitation patterns associated with the El Niño/Southern Oscillation. *Mon. Wea. Rev.*, **115,** 1606–1626.

——, and ——, 1989: Precipitation patterns associated with the high index phase of the Southern Oscillation. *J. Climate,* **3,** 268–284.

Streten, N. A., 1983: Southern Hemisphere circulation contrasts in the winters of 1972 and 1973. Preprints, *First Int. Conf. on Southern Hemisphere Meteorology,* São José dos Campos, São Paulo, Brazil, Amer. Meteor. Soc., 108–111.

Virji, H., 1981: A preliminary study of summertime tropospheric circulation patterns over South America estimated from cloud winds. *Mon. Wea. Rev.*, **109,** 599–610.

Weare, B. C., and J. S. Nasstrom, 1982: Examples of extended orthogonal function analysis. *Mon. Wea. Rev.*, **110,** 481–485.

Webster, P. J., 1972: Response of the tropical atmosphere to local steady forcing. *Mon. Wea. Rev.*, **100,** 518–541.

Weickmann, K. M., 1983: Intraseasonal circulation and outgoing longwave radiation modes during northern winter. *Mon. Wea. Rev.*, **111,** 1838–1858.

——, G. R. Lussky, and J. E. Kutzbach, 1985: A global-scale analysis of intraseasonal fluctuations of outgoing longwave radiation and 250-mb streamfunction during northern winter. *Mon. Wea. Rev.*, **113,** 941–961.